

SCIENTIFIC REPORTS



OPEN

Design of High Temperature Ti-Pd-Cr Shape Memory Alloys with Small Thermal Hysteresis

Received: 13 October 2015

Accepted: 01 June 2016

Published: 22 June 2016

Deqing Xue^{1,2}, Ruihao Yuan¹, Yumei Zhou¹, Dezhen Xue^{1,3}, Turab Lookman³, Guojun Zhang^{1,2}, Xiangdong Ding¹ & Jun Sun¹

The large thermal hysteresis (ΔT) during the temperature induced martensitic transformation is a major obstacle to the functional stability of shape memory alloys (SMAs), especially for high temperature applications. We propose a design strategy for finding SMAs with small thermal hysteresis. That is, a small ΔT can be achieved in the compositional crossover region between two different martensitic transformations with opposite positive and negative changes in electrical resistance at the transformation temperature. We demonstrate this for a high temperature ternary Ti-Pd-Cr SMA by achieving both a small ΔT and high transformation temperature. We propose two possible underlying physics governing the reduction in ΔT . One is that the interfacial strain is accommodated at the austenite/martensite interface via coexistence of B19 and 9R martensites. The other is that one of transformation eigenvalues equal to 1, i.e., $\lambda_2 = 1$, indicating a perfect coherent interface between austenite and martensite. Our results are not limited to Ti-Pd-Cr SMAs but potentially provide a strategy for searching for SMAs with small thermal hysteresis.

Shape memory alloys (SMAs) undergo a reversible martensitic phase transformation from the high symmetry austenite (A) to low symmetry martensite (M) phase upon the influence of temperature or stress field, giving rise to the shape memory effect (SME) and superelasticity (SE), respectively^{1,2}. Both thermally induced and mechanically induced martensitic transformations involve hysteresis, i.e., the forward and reverse martensitic phase transformations do not coincide^{3,4}. The hysteresis is the macroscopic manifestation of the dissipated energy during a phase transformation and it is generally considered to originate largely from the strain incompatibility at the A/M interface, which gives rise to an energy barrier for the phase transformation^{3,5,6}. During the cyclic thermal or mechanical martensitic phase transformation, strain incompatibility introduces several irreversible processes, such as the generation of dislocations and microcracks, resulting in serious fatigue^{7–9}. The fatigue degrades physical, mechanical properties of SMAs, especially the SME and SE, and finally leads to failure⁷. Therefore, the “reversibility”, the ability to pass back and forth through the phase transformation many times without degradation of properties, is critical and extensive research has focused on reducing hysteresis in order to improve the “reversibility” of SMAs^{3,4,10–13}.

In searching for thermoelastic SMAs with small thermal hysteresis (ΔT), several different methodologies have been utilized. Experimentally, combinatorial synthesis of SMA thin films has been employed to screen the various compositions and select the best candidates^{10,11,13,14}. Very recently, an adaptive design strategy based on machine learning algorithms has been shown to effectively explore the compositional space to identify alloys with very small hysteresis¹⁵. Theoretically, the geometrically non-linear theory of martensite (GNLTM) has been very useful in guiding the search for better alloys^{5,10}. The martensitic transformation can be described by the symmetric transformation matrix U , which maps the martensite lattice to the austenite lattice^{16,17}. The ordered eigenvalues of U , $\lambda_1 \leq \lambda_2 \leq \lambda_3$, represent the presence of an invariant habit plane between austenite and martensite^{16,17}. The GNLTM provides the constraint, $\lambda_2 = 1$, as means to reduce ΔT , so that there is a perfect coherent interface (unstressed and untwinned) between austenite and martensite⁵. Coupled with a combinatorial synthesis method, the GNLTM has led to the discovery of Ti-Ni-Cu and Ti-Ni-Cu-Pd systems with very small ΔT ^{10,14}. The

¹State Key Laboratory for Mechanical Behavior of Materials, Xi'an Jiaotong University, Xi'an 710049, China. ²School of Materials Science and Engineering, Xi'an University of Technology, Xi'an 710048, China. ³Theoretical Division, Los Alamos National Laboratory, Los Alamos, New Mexico 87545, USA. Correspondence and requests for materials should be addressed to D.X. (email: xuedezhen@mail.xjtu.edu.cn) or G.Z. (email: zhangguojun@xaut.edu.cn)

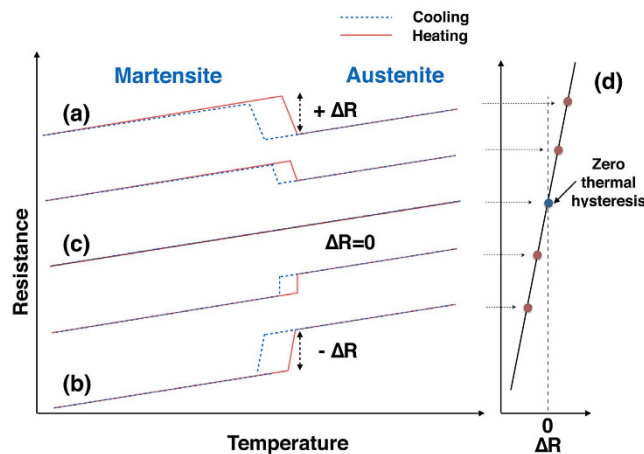


Figure 1. Schematic of the search strategy for SMAs with small thermal hysteresis. A martensitic transformation can result in (a) an increase of resistance ($+\Delta R$) from A to M, or (b) a drop in resistance $-\Delta R$, upon cooling. Therefore, (d) a crossover with $\Delta R=0$ can take place if ΔR varies with either defect doping or thermal treatment, (c) At the crossover condition, $\Delta R=0$, where the martensitic transformation can occur without any change in resistance upon cooling and heating, the alloy is presumed to have thermal hysteresis equal to zero.

correlation between $\lambda_2 = 1$ and ΔT has been confirmed for Ti-Ni-Au, Ti-Ni-Pt and Ti-Ni-Pd ternary systems by various authors^{5,18–20}.

However, the use of GNLT theory to design new SMAs requires *a priori* knowledge of crystal symmetry and lattice parameters, or the relationship between lattice parameters and alloying elements so that λ_2 can be evaluated in advance. The access of those information beforehand requires a lot of experimental efforts, especially for multicomponent systems. Thus, a simple strategy that can use the knowledge available to guide the design of SMAs with small ΔT is highly desirable.

In the present study, we propose that a compositional crossover region between two different types of martensitic transformations can give rise to small ΔT . Figure 1 shows our idea for designing new SMAs with small thermal hysteresis. Upon cooling, the martensitic transformation in some SMAs is accompanied by an increase in electrical resistance across the transformation from A to M (shown in Fig. 1(a) by $+\Delta R$), whereas in other SMAs the martensitic transformation is accompanied by a decrease in resistance at the martensitic transformation, as denoted in Fig. 1(b) by $-\Delta R$. Different martensites can be characterized by the distinct behavior they show with respect to ΔR . A $+\Delta R$ is due to the higher electrical resistance of M over A; and $-\Delta R$ indicates that M has a lower resistance than A. Examples of martensites with $+\Delta R$ include $\text{Ti}_{50}\text{Ni}_{50}$ (aged), $\text{Ti}_{50}\text{Ni}_{50-x}\text{Cu}_x$, $\text{Ti}_{50}\text{Ni}_{50-x}\text{Fe}_x$, $\text{Ti}_{50}\text{Pd}_{50-x}\text{Cr}_x$ ($x > 5\text{at.}$), whereas those with $-\Delta R$ include $\text{Ti}_{50}\text{Ni}_{50}$, $\text{Ti}_{50}\text{Ni}_{50-x}\text{Pd}_x$, $\text{Ti}_{50}\text{Pd}_{50-x}\text{Cr}_x$ ($x < 4\text{at.}$)²¹. It usually is the case that martensitic transformations with $+\Delta R$ can gradually change to those with $-\Delta R$ by either defect doping or thermal treatment^{21,22}. Therefore, we suggest that there exists a crossover so that a martensitic transformation can be accompanied without any change in resistance, i.e., $\Delta R=0$, as shown in Fig. 1(d). In another words, with ΔR continuously or monotonically varying with either defect doping or thermal treatment, there must exist a point or regime where $\Delta R=0$. In such a case, a martensitic transformation occurs without any change in resistance both on cooling and on heating, thus the thermal hysteresis would be expected to be zero (Fig. 1(c)).

We note that the energy dissipation (ΔT here) is much more severe in high temperature SMAs and as the transformation temperature increases, the thermal hysteresis should also increase dramatically. For example, $\text{Ti}_{50.0}\text{Ni}_{50.0}$ possesses a martensitic transformation temperature of 363 K and a ΔT of 30 K, whereas the ternary alloys Ti-Ni-Hf and Ti-Ni-Zr have higher transformation temperatures around 473 K and a much larger ΔT of 60 K. In the present study, we note that the Ti-Pd SMA system has a high martensitic transformation temperature, and more importantly, its martensitic transformation has the desirable feature of $+\Delta R$ and $-\Delta R$ depending on the different concentrations of defects. We thus demonstrate the key concept shown in Fig. 1 for the Ti-Pd-Cr SMAs by accomplishing both a small ΔT and a high transformation temperature. The functional stability from differential scanning calorimetry of our best alloy $\text{Ti}_{50}\text{Pd}_{45.3}\text{Cr}_{4.7}$ upon thermal cycling also significantly improved compared to the archetypal SMA $\text{Ti}_{50.0}\text{Ni}_{50.0}$. Our finding thus provides a straightforward strategy for searching for SMAs with small thermal hysteresis and high reversibility.

Results

To verify our strategy, we fabricated the $\text{Ti}_{50}\text{Pd}_{50-x}\text{Cr}_x$ system between 4 at.% and 5 at.% Cr. All the samples were fabricated in the present study under the exact same conditions to avoid the possible effects from microstructure and defects. We first checked the crystal structure of our samples. Typical X-ray diffraction profiles of all the samples are shown in Fig. 2(a). It is clear that all the diffraction peaks can be indexed by B19 martensite. However, it is also shown in the literature that the TiPd samples with high defect concentration, such as 5 at.% Cr, may possess 9R martensite structure as well²³. We further calculated the unit cell volume from our X-ray diffraction profiles

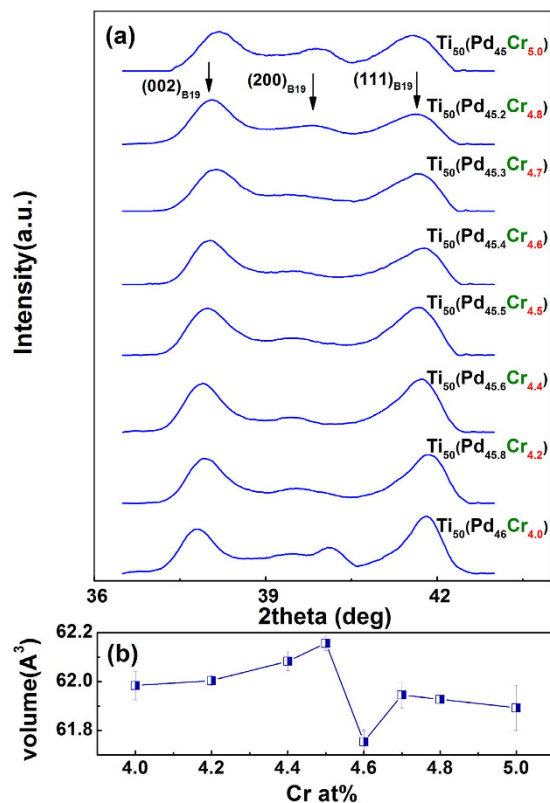


Figure 2. Crystal structure of $Ti_{50}Pd_{50-x}Cr_x$ SMAs system between 4 at.% Cr and 5 at.% Cr. (a) X-ray diffraction profiles show three typical peaks that can be indexed as $(002)_{B19}$, $(200)_{B19}$ and $(111)_{B19}$. (b) the calculated unit cell volume of samples with different Cr concentrations. A minimum of unit cell volume can be found at the 4.6 at.% Cr sample. The error bars were added by the fitting errors of the Bragg peaks.

and the result is shown in Fig. 2(b). A minimum unit cell volume occurs at 4.6 at.% Cr, indicating something special happens and will be discussed in the discussion part.

Figure 3 shows the resistance versus temperature ($R(T)$) curves of a number of compositions for the $Ti_{50}Pd_{50-x}Cr_x$ system between 4 at.% and 5 at.% Cr. $R(T)$ curves with $-\Delta R$ can be found in samples with Cr concentration near 4 at.%, and $R(T)$ curves with $+\Delta R$ are observed in samples with Cr concentration near 5 at.%. The former $-\Delta R$ situation corresponds to the B2 to B19 martensitic transformation that is typically found in $Ti_{50}Pd_{50}$ alloy, whereas the latter $+\Delta R$ is due to the B2 to 9R martensitic transformation which appears after heavily doping the $Ti_{50}Pd_{50}$ alloy with Cr, V, or Mn^{24,25}. For Cr concentration between 4.5 at.% and 4.7 at.%, the $R(T)$ curves do not possess the usual “S” shape at the transformation temperature, instead, show a tendency of flattening and merging together. Such evolution of ΔR from a positive value through almost zero to a negative value is exactly the situation expected in Fig. 1. According to the concept proposed in Fig. 1, alloys within this crossover composition range potentially possess very small ΔT .

Figure 4(a) shows how the thermal hysteresis ΔT varies with Cr concentration in $Ti_{50}Pd_{50-x}Cr_x$. The ΔT is calculated using $\Delta T = \frac{1}{2}(A_s + A_f - M_s - M_f)$, where M_s and M_f are the martensitic transformation start and finish temperatures, and A_s and A_f are the reverse transformation start and finish temperatures. These start and finish temperatures are determined using the tangent method as shown in the inset of Fig. 4(a). The ΔT is large for Cr concentration around 4.0 at.% with $-\Delta R$, and then decreases with increasing Cr concentration. It reaches a minimum at Cr concentration of 4.7 at.%, which is just within the composition crossover region mentioned above. ΔT then increases again for Cr concentration around 5.0 at.% with $+\Delta R$. We also determined ΔT from DSC measurements via endothermic and exothermic peaks, as shown in Fig. 4(b). The tangent method was employed to obtain A_s , A_f , M_s and M_f ; and ΔT was calculated using the same equation as for the $R(T)$ curves. The ΔT from DSC measurements behaves identically to that obtained from $R(T)$ curves, emphasizing the consistency of our approach. In addition to the tangent method, we also calculated ΔT from the exothermal/endothermic peak temperatures, $\Delta T = T_{exo} - T_{end}$, as shown in the left inset to Fig. 4(b). For this DSC measurement, we still see the characteristic “V” curve but with the smallest ΔT at 4.6 at.%, which is still in the crossover composition region. The “V” behavior in Fig. 4 is an experimental validation of our design recipe of Fig. 1.

Discussion

It is known that $+\Delta R$ and $-\Delta R$ correspond to the B2-B19 and B2-9R martensitic transformations, respectively. The optimized compositions just sit in the crossover region between B2-B19 and B2-9R transformations. Thus the optimal, smallest ΔT is likely to be due to instabilities associated with the three phases which include B2, B19

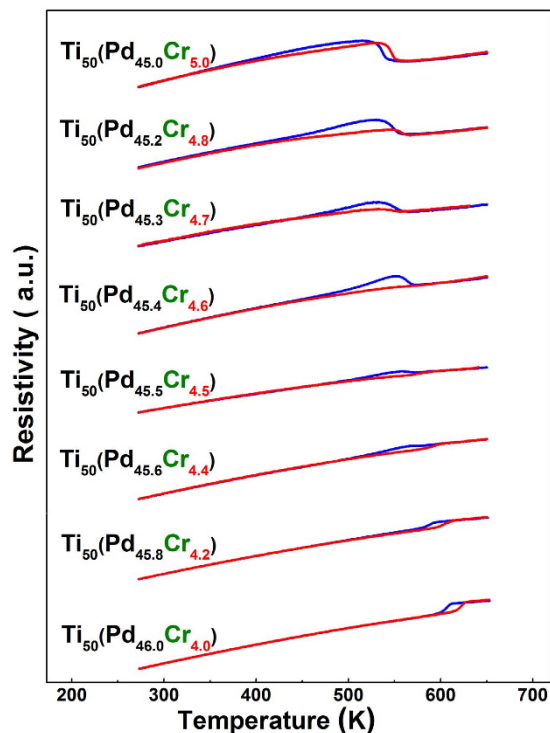


Figure 3. Experimental validation of our design recipe in $Ti_{50}Pd_{50-x}Cr_x$ SMAs. $R(T)$ curves for $Ti_{50}Pd_{50-x}Cr_x$ with different Cr concentrations are shown. The red line indicates the heating process while the blue one is the cooling curve. The $-\Delta R$ occurs at x around 4 at.%, and the $+\Delta R$ occurs at x around 5 at.%. Crossover region between 4.5 at.% and 4.7 at.% can give rise to narrow thermal hysteresis.

and 9R. At the phase transformation temperature in the crossover region, the three phases can be degenerate in energy, allowing the possibility of multiple transformation pathways. Most likely, the preferred pathway in the energy landscape is one that include a saddle point between the maxima of B19 and 9R. Microstructurally, the saddle point and pathway would correspond to coexisting B19 and 9R martensite at the A/M interface so that the strain at the A/M interface is easily accommodated via both B19 twins and 9R twins. However, for direct B2-B19 and B2-9R transformations, energy barriers need to be overcome for the phase transformations to take place. This is accompanied by larger strains at the habit planes for B2-B19 and B2-9R, resulting in larger ΔT . This explanation is consistent with the initial decrease in ΔT from a larger value to a fairly small value followed by an increase again to a relatively large value. Another possible physical origin relies on the eigenvalues of transformation strain matrix. Due to the strong correlation between $\lambda_2 = 1$ and small ΔT , it is also natural to expect that the samples with smallest ΔT , i.e., 4.6 at.% Cr and 4.7 at.% Cr, may possess $\lambda_2 = 1$. The abnormal unit cell volume change within 4 at.% and 5 at.% Cr shown in Fig. 2(b) may be supportive to this argument, as the λ_2 is closely related with the lattice parameters of martensite. Consequently, a perfect coherent interface (unstressed and untwinned) between austenite and martensite should be present in those TiPd samples with smallest ΔT . Although we provided two possible explanations for the low thermal hysteresis of our newly found alloy, the exact underlying mechanism still needs to be clarified in the future work.

The transformation hysteresis is known to be directly correlated with fatigue properties for SMAs. A smaller ΔT means that strain compatibility is satisfied relatively easily at the A/M interface and results in improved functional fatigue properties for SMAs cycled thermally. Thus, we investigated the functional stability of $Ti_{50}Ni_{50}$ and our best alloy, $Ti_{50}Pd_{45.3}Cr_{4.7}$, by thermal cycling using DSC. Figure 5 shows a compilation of 60 DSC cycles for the binary and ternary alloys. The shift of the DSC curves (transformation temperature) is about 13.5 K upon thermal cycling 60 times, as shown in Fig. 5(a). In contrast, the shift upon cycling is much less visible for our $Ti_{50}Pd_{45.3}Cr_{4.7}$ alloy (Fig. 5), and the inset highlights that the shift is only 2 K. Thus, we significantly improve the functional fatigue properties of our $Ti_{50}Pd_{45.3}Cr_{4.7}$ alloy via the design strategy in Fig. 1.

Our new alloy does not only have a very small thermal hysteresis, it also possesses a very high transition temperature. Figure 6 compares our results with those reported previously, which is beneficial in the search for high temperature SMAs with small hysteresis and high reversibility^{3,14,26}. We observe that the Au-Cu-Zn and Ti-Ni-Cu-Pd alloys exhibit not only the smallest thermal hysteresis, but also low transformation temperatures. For traditional high temperature SMAs, such as Ti-Ni-Hf, Ti-Ni-Zr, the thermal hysteresis always reaches 30 K or more, indicating poor functional fatigue. Using our design strategy, the $Ti_{50}Pd_{45.3}Cr_{4.7}$ alloy attains a superior combination of both small thermal hysteresis and high transformation temperature than other high temperature alloys.

In summary, we have proposed a design strategy for finding new SMAs with small thermal hysteresis. That is, a small ΔT can be achieved in the crossover region between two martensitic transformations with opposite changes

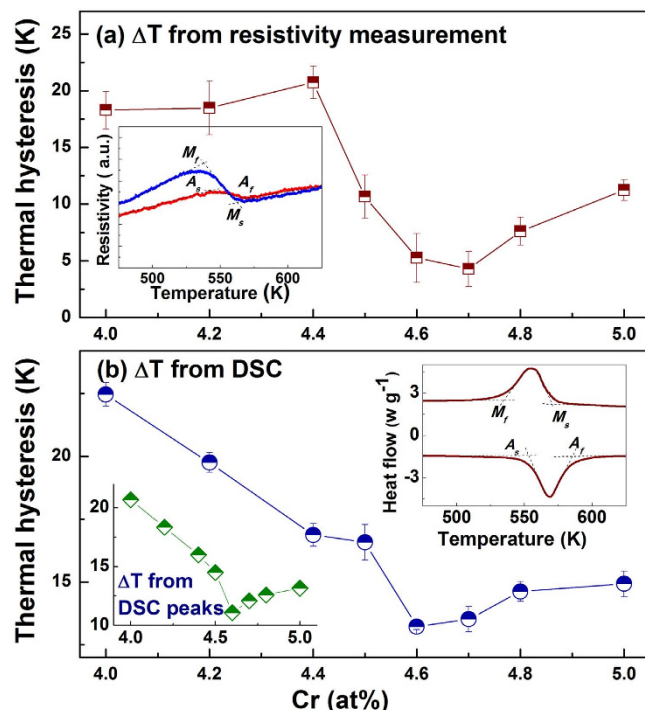


Figure 4. The behavior of the thermal hysteresis ΔT as a function of concentration is consistent with our notion that small ΔT occurs in the crossover region for $Ti_{50}Pd_{50-x}Cr_x$. (a) $\Delta T = \frac{1}{2}(A_s + A_f - M_s - M_f)$ from R(T) measurements, where A_s, A_f, M_s and M_f are determined by the tangent method (inset). (b) $\Delta T = \frac{1}{2}(A_s + A_f - M_s - M_f)$ from DSC measurements, where A_s, A_f, M_s and M_f are determined using the tangent method (right corner inset). The ΔT directly determined by exothermal/endothermic peak temperatures are shown in the left corner inset, revealing the same behavior. The error bars were determined by choosing the start and finish temperatures (A_s, A_f, M_s and M_f) for several times employing the tangent method.

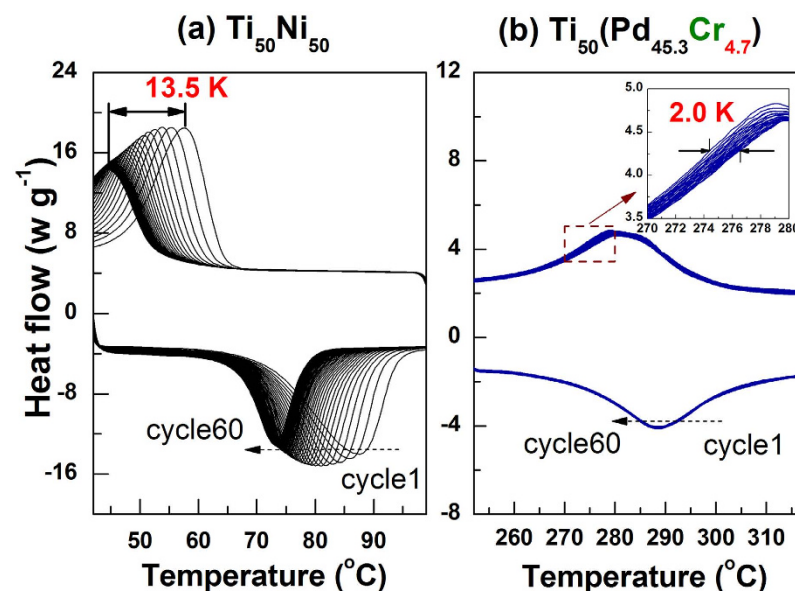


Figure 5. Functional fatigue behavior of bulk alloys. Compilation of 60 DSC cycles plotted for (a) $Ti_{50}Ni_{50}$, (b) $Ti_{50}Pd_{45.3}Cr_{4.7}$. The inset in (b) enlarges the shift of the DSC curves for $Ti_{50}Pd_{45.3}Cr_{4.7}$. The shift in $Ti_{50}Ni_{50}$ of 13.5 K is much larger than that in $Ti_{50}Pd_{45.3}Cr_{4.7}$ of 2.0 K, indicating a significant improvement in functional fatigue.

in electrical resistance at the transformation temperature. By using this, we find that the alloy $Ti_{50}Pd_{45.3}Cr_{4.7}$ possess both very small thermal hysteresis and high transformation temperature. Moreover, Cr is not the only dopant that can be used to vary ΔR . The alloy families Ti-Pd-V, Ti-Pd-Mn, Ti-Pd-Ni are potentially promising systems

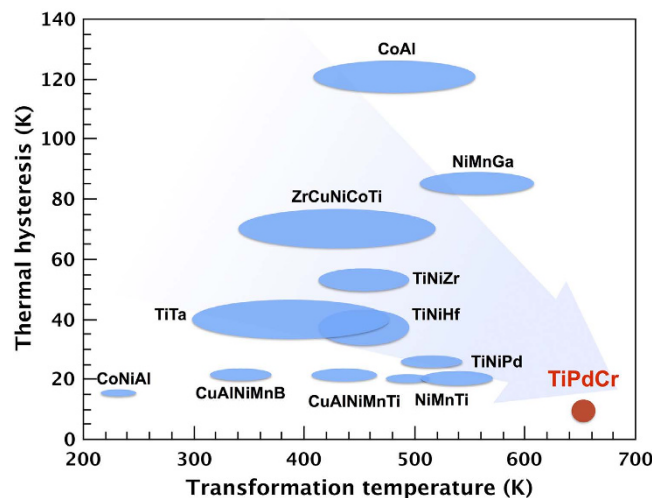


Figure 6. A comparison of the thermal hysteresis and transformation temperature for the bulk SMAs. The thermal hysteresis and transformation temperature values of CoAl²⁷, ZrCuNiCoTi²⁸, NiMnGa^{29,30}, TiNiHf³¹, TiNiPd^{32,33}, TiNiZr^{34,35}, TiTa³⁶, CoNiAl³⁷, ZnAuCu³, CuAlNiMnB³⁸, TiNiCuPd¹⁴, CuAlNiMnTi²⁶, and NiMnTi³⁹ are collected from literatures.

likely to show similar behavior. Thus, we expect the present design strategy to guide the discovery of new SMAs with small ΔT by either doping or thermal treatment.

Methods

Base ingots of $Ti_{50}Pd_{50-x}Cr_x$ ($x = 4.0, 4.2, 4.4, 4.5, 4.6, 4.7, 4.8, 5.0 at\%$) alloys were made by arc melting a mixture of 99.9% pure Ti, 99.9% pure Pd and 99.9% pure Cr in an argon atmosphere. Specimens for measurement were spark cut from the ingots that were hot rolled to 1 mm thick. They were then solution treated at 1273 K for 1 hour in evacuated quartz tubes and quenched into ice water. In order to remove the affected surface layer, the specimens were mechanically polished, and followed by chemical etching.

A temperature dependent resistance ($R(T)$) measurement was made with a cooling/heating rate of $2 Kmin^{-1}$ to detect the resistance change ($+\Delta R$ or $-\Delta R$) at the martensitic transformation. Differential scanning calorimetry (DSC) measurements were also employed with a cooling/heating rate of $10 Kmin^{-1}$ to measure the martensitic transformation by exothermal/endothermic peaks.

References

- Otsuka, K. & Wayman, C. *Shape Memory Materials* (Cambridge University Press, 1999).
- Otsuka, K. & Kakeshita, T. Science and technology of shape-memory alloys: new developments. *MRS Bulletin* **27**, 91–100 (2002).
- Song, Y., Chen, X., Dabade, V., Shield, T. W. & James, R. D. Enhanced reversibility and unusual microstructure of a phase-transforming material. *Nature* **502**, 85–88 (2013).
- Chluba, C. *et al.* Ultralow-fatigue shape memory alloy films. *Science* **348**, 1004–1007 (2015).
- Zhang, Z., James, R. D. & Müller, S. Energy barriers and hysteresis in martensitic phase transformations. *Acta Mater.* **57**, 4332–4352 (2009).
- Gröger, R., Lookman, T. & Saxena, A. Defect-induced incompatibility of elastic strains: dislocations within the Landau theory of martensitic phase transformations. *Phys. Rev. B* **78**, 184101 (2008).
- Eggeler, G., Hornbogen, E., Yawny, A., Heckmann, A. & Wagner, M. Structural and functional fatigue of NiTi shape memory alloys. *Mater. Sci. Eng.: A* **378**, 24–33 (2004).
- Norfleet, D. *et al.* Transformation-induced plasticity during pseudoelastic deformation in Ni-Ti microcrystals. *Acta Mater.* **57**, 3549–3561 (2009).
- Simon, T., Kröger, A., Somsen, C., Dlouhy, A. & Eggeler, G. On the multiplication of dislocations during martensitic transformations in NiTi shape memory alloys. *Acta Mater.* **58**, 1850–1860 (2010).
- Cui, J. *et al.* Combinatorial search of thermoelastic shape-memory alloys with extremely small hysteresis width. *Nat. Mater.* **5**, 286–290 (2006).
- Buenconsejo, P. J. S. *et al.* A new prototype two-phase (TiNi)-(β - ω) SMA system with tailorable thermal hysteresis. *Adv. Funct. Mater.* **21**, 113–118 (2011).
- König, D. *et al.* Thickness-dependence of the B2-B19 martensitic transformation in nanoscale shape memory alloy thin films: Zero-hysteresis in 75 nm thick $Ti_{51}Ni_{38}Cu_{11}$ thin films. *Acta Mater.* **60**, 306–313 (2012).
- Buenconsejo, P. J. S. & Ludwig, A. New Au-Cu-Al thin film shape memory alloys with tunable functional properties and high thermal stability. *Acta Mater.* **85**, 378–386 (2015).
- Zarnetta, R. *et al.* Identification of Quaternary Shape Memory Alloys with Near-Zero Thermal Hysteresis and Unprecedented Functional Stability. *Adv. Funct. Mater.* **20**, 1917–1923 (2010).
- Xue, D. *et al.* Accelerated search for materials with targeted properties by adaptive design. *Nat. Comm.* **7**, 11241 (2016).
- Lieberman, D. S., Wechsler, M. & Read, T. Cubic to orthorhombic diffusionless phase change—experimental and theoretical studies of AuCd. *J. Appl. Phys.* **26**, 473–484 (1955).
- Bhattacharya, K. *Microstructure of Martensite: Why it Forms and how it Gives Rise to the Shape-memory Effect*. Oxford Series on Materials Modelling (OUP Oxford, 2003).
- Chen, X., Srivastava, V., Dabade, V. & James, R. D. Study of the cofactor conditions: Conditions of supercompatibility between phases. *J. Mech. Phys. Solid.* **61**, 2566–2587 (2013).

19. Shi, H., Delville, R., Srivastava, V., James, R. & Schryvers, D. Microstructural dependence on middle eigenvalue in Ti-Ni-Au. *J. Alloys Compd.* **582**, 703–707 (2014).
20. Delville, R. *et al.* Transmission electron microscopy study of phase compatibility in low hysteresis shape memory alloys. *Philos. Mag.* **90**, 177–195 (2010).
21. Otsuka, K. & Ren, X. Physical metallurgy of Ti-Ni-based shape memory alloys. *Prog. Mater. Sci.* **50**, 511–678 (2005).
22. Zhou, Y. *et al.* Origin of 2-stage R-phase transformation in low-temperature aged Ni-rich Ti-Ni alloys. *Acta Mater.* **53**, 5365–5377 (2005).
23. Enami, K. & Nakagawa, Y. R martensite in the Ti-Pd-Fe alloys. *Proc. ICOMAT (1992)*. 521–526 (1993).
24. Enami, K., Hori, K. & Takahashi, J. Martensitic transformation in TiPd-Cr alloys. *ISIJ Int.* **29**, 430–437 (1989).
25. Enami, K. & Hoshiya, T. Development of high temperature shape memory materials. *ISIJ Int.* **8**, 361–370 (1993).
26. Ma, J., Karaman, I. & Noebe, R. D. High temperature shape memory alloys. *Int. Mater. Rev.* **55**, 257–315 (2010).
27. Omori, T., Sutou, Y., Oikawa, K., Kainuma, R. & Ishida, K. Shape memory effect in the ferromagnetic Co-14 at.% alloy. *Scripta Mater.* **52**, 565–569 (2005).
28. Firstov, G., Van Humbeeck, J. & Koval, Y. N. Comparison of high temperature shape memory behaviour for ZrCu-based, Ti-Ni-Zr and Ti-Ni-Hf alloys. *Scripta Mater.* **50**, 243–248 (2004).
29. Li, Y., Xin, Y., Jiang, C. & Xu, H. Shape memory effect of grain refined $Ni_{54}Mn_{25}Ga_{21}$ alloy with high transformation temperature. *Scripta Mater.* **51**, 849–852 (2004).
30. Xin, Y., Li, Y., Chai, L. & Xu, H. Shape memory characteristics of dual-phase Ni-Mn-Ga based high temperature shape memory alloys. *Scripta Mater.* **57**, 599–601 (2007).
31. Meng, X., Zheng, Y., Cai, W. & Zhao, L. Two-way shape memory effect of a TiNiHf high temperature shape memory alloy. *J. Alloys Compd.* **372**, 180–186 (2004).
32. Golberg, D. *et al.* Characteristics of $Ti_{50}Pd_{30}Ni_{20}$ high-temperature shape memory alloy. *Intermetallics* **3**, 35–46 (1995).
33. Liu, Y., Kohl, M., Okutsu, K. & Miyazaki, S. A tinipd thin film microvalve for high temperature applications. *Mater. Sci. Eng., A* **378**, 205–209 (2004).
34. Hsieh, S. & Chang, W. Martensitic transformation of an aged/thermal-cycled $Ti_{30.5}Ni_{49.5}Zr_{10}Hf_{10}$ shape memory alloy. *J. Mater. Sci.* **37**, 2851–2856 (2002).
35. Sawaguchi, T., Sato, M. & Ishida, A. Grain-size effect on shape-memory behavior of $Ti_{35.0}Ni_{49.7}Zr_{15.4}$ thin films. *Metall. Mater. Trans. A* **35**, 111–119 (2004).
36. Buenconsejo, P. J. S., Kim, H. Y., Hosoda, H. & Miyazaki, S. Shape memory behavior of Ti-Ta and its potential as a high-temperature shape memory alloy. *Acta Mater.* **57**, 1068–1077 (2009).
37. Karaca, H., Karaman, I., Lagoudas, D., Maier, H. & Chumlyakov, Y. I. Recoverable stress-induced martensitic transformation in a ferromagnetic CoNiAl alloy. *Scripta Mater.* **49**, 831–836 (2003).
38. Morris, M. High temperature properties of ductile CuAlNi shape memory alloys with boron additions. *Acta Metall.* **40**, 1573–1586 (1992).
39. Potapov, P. Martensitic transformations and high-temperature shape memory effect in the intermetallic NiMn alloyed with Ti. *Met. Sci. Heat Treat.* **35**, 520–525 (1993).

Acknowledgements

The authors gratefully acknowledge the support of National Basic Research Program of China (Grant No. 2012CB619401), the National Natural Science Foundation of China (Grant Nos 51571156, 51321003, 51571156, 51302209, 51431007, and 51320105014), and 111 project of China (B06025). XD and TL are also grateful to the LDRD-DR program at Los Alamos National Laboratory for support.

Author Contributions

D.Z.X. and G.Z. designed the research project. D.Q.X. wrote the initial draft. D.Q.X., R.Y. and Y.Z. performed all the experiments. T.L., X.D. and J.S. provided valuable comments and suggestions to the work. All authors contributed to the writing of the paper.

Additional Information

Competing financial interests: The authors declare no competing financial interests.

How to cite this article: Xue, D. *et al.* Design of High Temperature Ti-Pd-Cr Shape Memory Alloys with Small Thermal Hysteresis. *Sci. Rep.* **6**, 28244; doi: 10.1038/srep28244 (2016).



This work is licensed under a Creative Commons Attribution 4.0 International License. The images or other third party material in this article are included in the article's Creative Commons license, unless indicated otherwise in the credit line; if the material is not included under the Creative Commons license, users will need to obtain permission from the license holder to reproduce the material. To view a copy of this license, visit <http://creativecommons.org/licenses/by/4.0/>